Self-organized criticality involving vector fields and random driving

P. A. Robinson
School of Physics, University of Sydney, New South Wales 2006, Australia
(Received 11 May 1993)

The effects of vector fields and random driving on the self-organized critical state are investigated using cellular-automaton simulations and scaling arguments. It is found that the vector-field dynamics are very similar to those for the scalar-field case: one field component dominates the evolution for a wide range of parameters, with the other components slaved to it. The self-organized critical state is also found to be extremely robust with respect to randomness in the driving, but it eventually breaks down when randomization destroys the critical correlations faster than they can be established.

PACS number(s): 05.50.+q, 05.70.Jk, 05.90.+m

I. INTRODUCTION

Bak *et al.* [1] proposed the concept of self-organized criticality (SOC) to explain the widespread occurrence of scale-invariant, power-law correlations in nature, as typified by $1/f$ noise. Since it was first recognized in a model of avalanches in sandpiles, SOC has been applied to phenomena ranging from forest fires to electrical noise and earthquakes and the basic sandpile-type model has proved to be particularly versatile. This model illustrates the emergence of a unique critical state in which there exists a statistical balance between instability due to driving (e.g., via addition of sand grains for sandpiles), and relaxation (e.g., via avalanches in sandpiles) when instability sets in. This state exhibits power-law correlations in space and time.

Many authors have carried out cellular-automaton simulations of the properties of the model of Bak and coworkers [1–8], or analytic calculations involving it or its continuum counterparts [3,4,9–11]. Many physical systems involve vector fields. However, virtually all work on self-organized criticality to date has been concerned with the scalar case. The one example of vector-field SOC considered in the literature involved the buildup of magnetic energy in the solar corona, balanced by release in solar flares [12], but the properties of vector-field SOC have not been considered in any detail to date. In a similar vein, most work on SOC has involved discrete models for which the field takes on one of a few (usually two or four) integer values. Zhang [4] showed that continuously-valued fields display very similar and robust behavior. In his work the SOC state persisted even when the size of the grains added to the sandpile was a random variable. He argued that randomness in the driving was relatively unimportant, but did not explore this point in detail to determine the limits of SOC behavior.

In this paper we investigate the properties of the SOC state for a sandpile-type model, concentrating on the effects of vector fields and randomized driving in two-dimensional systems. In Sec. II we define the model discussed in this work. Section III is then concerned with investigating the properties of scalar SOC and comparing them with the vector case. Finally, in Sec. IV, we investigate the robustness of SOC as the secular component of the driving (the mean grain size for sandpiles) is decreased relative to the random part (randomness in the grain size for sandpiles).

II. THE MODEL

The model investigated here involves a D-component vector field $\mathbf{h}$ defined on a two-dimensional square grid. The driving step consists of adding a field increment ("sand grain") $\mathbf{g}$ to a randomly chosen site, labeled (i,j), with

$$\mathbf{h}(i,j) \rightarrow \mathbf{h}(i,j) + \mathbf{g}. \tag{1}$$

The increment $\mathbf{g}$ is a random variable, with the mean satisfying

$$\langle g_j \rangle = \begin{cases} \mu, & j = 1, \\ 0, & j > 1. \end{cases} \tag{2}$$

Each component of $\mathbf{g}$ also has an additive random part uniformly distributed between $-\Delta$ and Δ. The choice of g_1 to be the only component with a nonzero mean does not imply any loss of generality because the coordinates defining the field components can always be rotated to bring $\langle \mathbf{g} \rangle$ into the form given by (2).

Relaxation occurs when the addition of a grain causes $h(i,j) = |\mathbf{h}(i,j)|$ to exceed a critical value, which we set equal to unity without loss of generality. The field at the site (i,j) then relaxes to zero, with its original value being equally distributed to its four nearest neighbors, thereby conserving $\mathbf{h}$ in this step. Some of these neighbors may then become unstable and relax in turn (with all unstable sites relaxing simultaneously), followed by relaxations of more distant sites. Relaxation is allowed to proceed until all sites are stable before the next height increment is added. The *size* s of the avalanche is defined to be the total number of different sites to undergo relaxation, while the *activation number* a is the total number of relaxations, accounting for multiple relaxations at a

given site. The triggering condition $|h| > 1$ used here is slightly different from the condition $h > 1$ (or a close analog) used in previous works on scalar fields. This modification is necessary to treat the vector case, but makes little difference for scalar fields, except for $\mu \approx 0$ (see Sec. IV).

The (open) boundary condition used is that $\mathbf{h}(i,j) = \mathbf{0}$ for all sites on the edge of the grid. In the case of a sandpile, this implies that grains that reach the edge fall off and leave the pile, thereby enabling a statistically steady state to be attained.

One point that is worth noting is that in this model it is the magnitude ("height") of the field that determines instability, rather than the slope, as would be expected for a sandpile. Bak *et al.* [1,2], for example, originally introduced a height function as a simple proxy for the mean slope, not to represent the height directly. This has the advantage of numerical speed and simplicity, although the true height of the pile is not uniquely determined by the mean-slope values, except in one dimension.

III. THE SOC STATE

The first part of our analysis is to establish that the model under consideration displays self-organized criticality, and to investigate the properties of this state, comparing them with results obtained by previous authors. Scalar SOC is considered in Sec. III A, while the vector case appears in Sec. III B.

A. Scalar self-organized criticality

A system of size $N \times N$, with $N = 200$ and $D = 1$, was driven by adding increments with $\mu = 0.16$ and $\Delta = 0.4$ until it reached a statistically steady state. Figure 1(a) shows the subsequent distribution $D(s)$ of avalanche sizes s in this state. This distribution is seen to be a power law over approximately three decades, truncated by finite-size effects above $s \approx 10^{3.5}$, with

$$D(s) \sim s^{1-\tau}, \tag{3}$$

and $\tau \approx 2.23 \pm 0.05$ for $s < 10^{3.5}$. The power-law statistics are indicative of self-organized criticality. Figure 1(b) shows the distribution $D(a)$ of activation numbers a. This is seen to be a power-law over four decades, with

$$D(a) \sim a^{1-\alpha}, \tag{4}$$

and $\alpha = 2.25 \pm 0.05$ for $a < 10^{4.5}$.

A scatter plot of a vs s is shown in Fig. 1(c). For $s \lesssim 100$, $a \approx s$ is satisfied, subject to the strict inequality $a \geq s$. However, for $s \gtrsim 300$, the scatter plot changes slope, with

$$a \sim s^{\delta_a}, \tag{5}$$

and $\delta_a = 1.52 \pm 0.10$. Comparison with systems of different sizes shows that this change in behavior is *not* a finite-size effect, since the breakpoint is independent of N and occurs for s below the point where finite-size effects truncate $D(s)$. Physically, the transition occurs at the point at which multiple activations of individual sites first become important: for small avalanches such reactivations are unimportant and transport is directed chiefly outward from the initial unstable site, but they dominate at large s where $a \gg s$ is satisfied. Equations (3)–(5) imply that δ_a, τ, and α are related, with

$$\alpha = 2 + (\tau - 2)/\delta_a. \tag{6}$$

This result means that the breakpoint in Fig. 1(b) should correspond to a breakpoint in Fig. 1(c). The predicted change in α from 2.23 to 2.15 as a increases is not clearly distinguishable, given the uncertainties, but there is a slight reduction in slope for $3.5 \lesssim \log_{10} a \lesssim 4.5$.

The values of τ and α determined above lie toward the upper end of the range 2.0 ± 0.1 to 2.2 ± 0.1 of estimates obtained for similar systems by other authors [1,4–8,10], concurring reasonably well with the numerical estimate $\tau = 2.22$ by Manna [7] and the dynamical renormalization group result $\tau = 13/6$ [10]. Zhang argued for $\tau = 2$ assuming that all avalanches locally transfer equal amounts of energy, regardless of size [4]. This prediction is not borne out for the present model; however, we note that Christensen *et al.* [8] showed that slight changes to the driving and/or boundary conditions can shift exponents for a similar (but discrete) model within the range 2.0 to 2.2.

In the SOC state, we find the mean of h_1 to be $\langle h_1 \rangle = 0.62 \pm 0.01$ for a wide range of values of μ and Δ, discussed further in Sec. IV, in excellent agreement with Zhang's result for a similar model [4]. Figure 2(a) shows the distribution $D(h_1)$ of h_1 in the SOC state, again for $N = 200$, $\mu = 0.16$, and $\Delta = 0.4$. As noted by Zhang for his model [4], a series of narrow peaks are seen at $h_1 = 0$, 0.31, 0.62, 0.93, despite the randomness in the

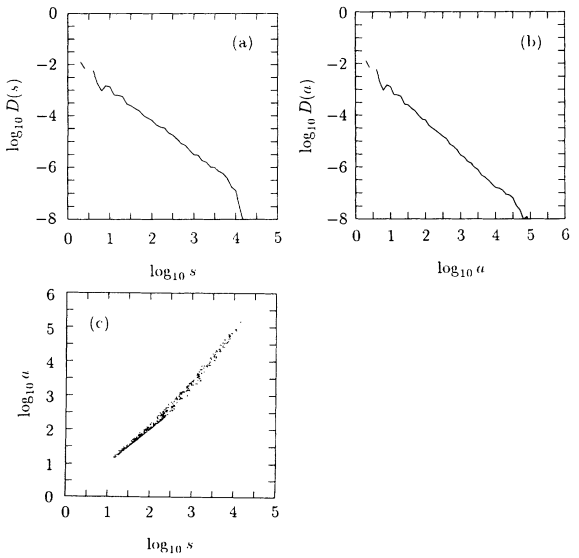

FIG. 1. Self-organized critical state in a system with $D = 1$, $\mu = 0.16$, $\Delta = 0.4$, and $N = 200$. (a) Distribution $D(s)$ of avalanche sizes vs s. (b) Distribution $D(a)$ of activation numbers vs a. (c) Scatter plot of a vs s for several thousand avalanches.

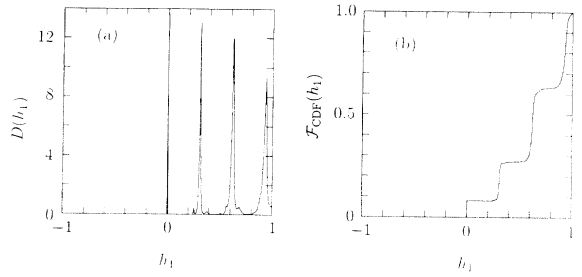

FIG. 2. SOC distribution and CDF of h_1 for the same system as in Fig. 1. (a) Distribution $D(h_1)$ of h_1. (b) Cumulative distribution $\mathcal{F}_{\rm CDF}(h_1)$ of h_1.

driving. Zhang [4] developed a theory for these peaks. Generalizing to vector fields, his argument was that a given site receives increments in h_1 of size q each time one of its neighbors relaxes during an avalanche, thereby leading to the observed peaks. Here we note that unstable sites redistribute their $\mathbf{h}$ values equally to their $2d$ nearest neighbors as soon as they pass the instability threshold $|\mathbf{h}| = 1$. This implies

$$(2d-1)q < 1 < 2dq. \tag{7}$$

Values of q toward the extremes of this range will tend to be eliminated as avalanches mix together contributions from various sites. Hence, taking an average of (7), we find

$$q \approx \frac{4d-1}{4d(2d-1)}. \tag{8}$$

For $d = 2$, this yields $q \approx 0.29$, in good agreement with the observed value of 0.31.

Figure 2(b) shows the cumulative distribution function

$$\mathcal{F}_{\rm CDF}(h_1) = \int_{-1}^{h_1} D(h_1')dh_1', \tag{9}$$

as a function of h_1. It is seen that a negligible number of sites have $h_1 < 0$, even though Δ exceeds μ in the driving. The implication is that avalanches rapidly eliminate negative values of h_1 as they organize the system into the critical height distribution shown in Fig. 2(a). Most of the sites are clustered around the sharp peaks in $D(h_1)$, as was noted for Zhang's model [4], with fractions 0.08, 0.19, 0.36, and 0.37 in the four peaks (in order of increasing h_1). These values are consistent with those of Zhang [4] who found corresponding fractions of 0.10, 0.16, 0.32, and (correcting an apparent typographical error) 0.42. Analytical calculations on a discrete model of SOC [11] yielded a value of 0.074 for the first peak, and results which we find to be consistent with the ranges 0.13–0.31, 0.13–0.40, and 0.31–0.66 for the other three peaks, respectively. These values are all consistent with our numerical results for continuously-valued fields.

B. Vector self-organized criticality

A simulation with a two-component field ($D = 2$) for $N = 200$, $\mu = 0.16$, and $\Delta = 0.4$ yields results nearly identical to those in Fig. 1 for $D = 1$. In particular, the results $\tau = 2.22 \pm 0.05$, $\alpha = 2.27 \pm 0.05$, $\delta_a = 1.55 \pm 0.10$, and $\langle h_1 \rangle = 0.62 \pm 0.01$ are all the same as for $D = 1$ to within their uncertainties. The distribution of h_1 was also found to be very similar to that shown in Fig. 2(a) for the case $D = 1$, the only noticeable differences being slight changes in the heights of the various peaks, while the fractions of sites corresponding to the peaks remain essentially constant. These results imply that the behavior of the SOC state is dominated by the evolution of h_1, which proceeds as for $D = 1$ for the parameters considered.

If the SOC dynamics are indeed dominated by the behavior of h_1, the scaling of $\sigma(h_2)$ can be related to transport in the system by the following argument: The mean rate of increase in $\langle h_1 \rangle$ (per added increment) due to addition of field increments is proportional to μ. In the SOC state, this must be balanced on average by losses, which thus satisfy

$$\frac{d\langle h_1 \rangle}{dn} \propto -\mu. \tag{10}$$

The form of the relaxation mechanism ensures that transport of h_2^2 proceeds in tandem with transport of h_1, because all components of $\mathbf{h}$ relax together at each unstable site. Hence, in parallel with (10), we find losses of

$$\frac{d\langle h_2^2 \rangle}{dn} \propto -\mu \frac{\langle h_2^2 \rangle}{\langle h_1 \rangle}. \tag{11}$$

These losses must balance the rate of input of $\langle h_2^2 \rangle$, which is proportional to Δ^2, giving

$$\langle h_2^2 \rangle \propto \Delta^2/\mu. \tag{12}$$

Figure 3 shows $\sigma(h_2)$, the RMS value of h_2, as a function of $1/N$ for $20 \le N \le 200$ for $\mu = 0.08$ and $\Delta = 0.2$. Extrapolation of the observed linear trend yields $\sigma(h_2) = \langle h_2^2 \rangle^{1/2} = 0.012 \pm 0.001$ in the limit $N \to \infty$. The scalings of $\sigma(h_2)$ with μ and Δ are explored in Fig. 4 for $N = 100$ and $D = 2$. Combining these results, we find

$$\sigma^2(h_2) \approx 3 \times 10^{-4} \frac{\Delta^{1.98 \pm 0.02}}{\mu^{1.01 \pm 0.03}}, \tag{13}$$

for $N \to \infty$, with the scalings being in reasonable agreement with (12). The uncertainties in (13) are those of the least-squares fit to the data points shown.

Figure 5 shows the variation of τ, $\langle h_1 \rangle$, and

$$\sigma = \left(\frac{1}{D-1} \sum_{j=2}^{D} \sigma^2(h_j) \right)^{1/2}, \tag{14}$$

as functions of D for systems with $\mu = 0.16$, $\Delta = 0.4$, $N = 40$, and $D = 1$, 2, 3, 4, 6, 10, 15, and 20. There is little if any variation in τ with D, while $\langle h_1 \rangle$ decreases slowly as D increases. Contrastingly, σ falls more steeply, but the RMS total of all the components other than h_1 continues to increase, with $(D-1)^{1/2}\sigma \approx 0.21$ at $D = 20$. The constancy of τ implies that the SOC state survives for the entire range of D investigated, despite the changes in its mean parameters. Similar results for $D = 1$, 2, 3,

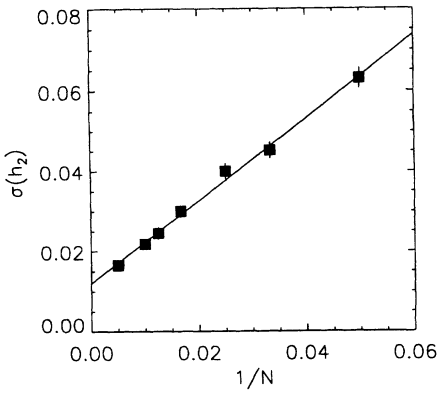

FIG. 3. RMS value of h_2, $\sigma(h_2)$, for $D = 2$, $\mu = 0.16$, $\Delta = 0.4$, as a function of $1/N$. The solid curve is the line of best fit.

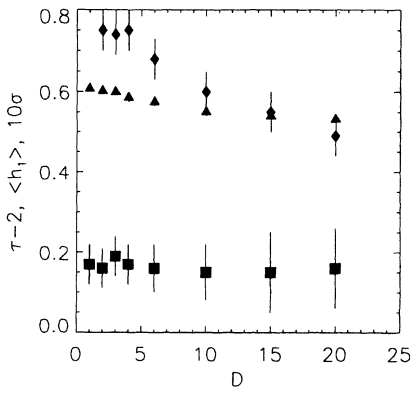

FIG. 5. Dependence of the SOC state on D. Squares show $\tau - 2$, triangles show $\langle h_1 \rangle$, and diamonds show 10σ [cf. Eq. (14)].

6 were obtained for the same parameters with $N = 100$.

Figure 6 shows the h_1 distributions for the $D = 1$, 2, 6, and 20 simulations from Fig. 5. In Fig. 6(a) we see the four peaks first noted by Zhang [4]. As expected from Sec. III A, Fig. 6(b) shows no sharp change with respect to the scalar case. As D increases further, in Figs. 6(c) and 6(d), the three peaks with $h_1 > 0$ broaden slowly and decrease in height, while their separation also decreases slightly. However, we find that the proportions of sites corresponding to the peaks remain virtually unchanged. Two differences between cases $D = 1$ and $D \gg 1$ are that the peak separation q decreases slowly with D, and the number of sites with h_1 close to 1 decreases owing to the decreasing fraction of parameter space corresponding to $h_1 \approx 1$.

From the results in Figs. 5 and 6 we conclude that the SOC state persists for vector fields, with its properties changing only very slowly with D.

IV. EFFECTS OF RANDOM DRIVING

In the limit $\mu \to 0$ we expect the random part of the driving Δ to swamp the secular part, destroying SOC.

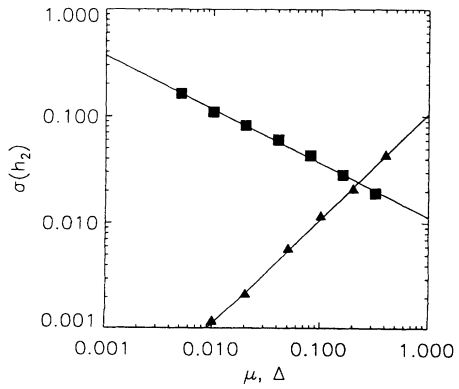

FIG. 4. Dependence of $\sigma(h_2)$ on Δ (triangles) and μ (squares) for $D = 2$ and $N = 100$. The value of μ is fixed at 0.08 when determining the Δ dependence, while $\Delta = 0.4$ is fixed for the μ dependence. Solid curves are lines of best fit.

This limit is investigated in this section.

A. Scalar case

One measure of the randomness in g is the ratio χ of the number, $1/\mu$, of secular increments required to trigger relaxation at a site with $h = 0$ initially to the typical number, $3/\Delta^2$, for random diffusion to bring about the same outcome, giving

$$\chi = \Delta^2/3\mu. \tag{15}$$

The quantity χ is also important in determining $\sigma(h_j)$ for $j > 1$ (see Eq. (12)], with the data in Fig. 4 collapsing onto a single line when plotted as a function of χ.

In Fig. 7 we plot $\langle h_1 \rangle$ and the standard deviation $\sigma(h_1)$ as functions of χ for $D = 1$, $\Delta = 0.4$, $N = 100$, and $0 \leq \mu \leq 0.32$. The results show little change for $\chi \lesssim$

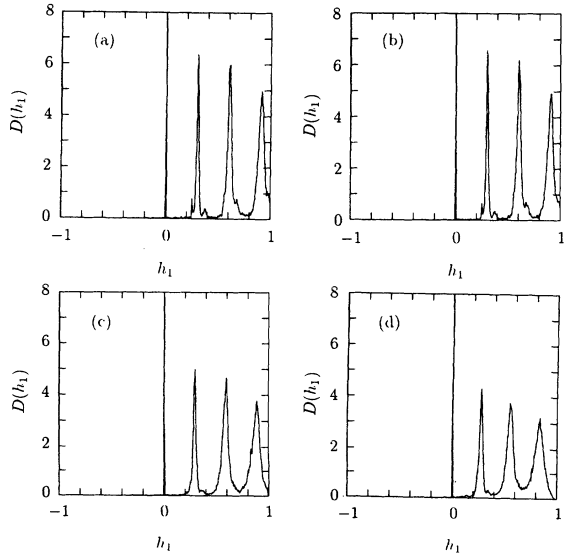

FIG. 6. Height distributions in the SOC state for $\mu = 0.08$, $\Delta = 0.4$, $N = 40$. (a) $D = 1$. (b) $D = 2$. (c) $D = 6$. (d) $D = 20$.

100, indicating the existence of an essentially unique SOC state. For $\chi \gtrsim 100$, there is a steady change in this SOC state, with $\langle h_1 \rangle$ decreasing and $\sigma(h_1)$ increasing with χ. Figure 8(a) shows $D(h_1)$ for $\chi = 267$ and $N = 100$ from Fig. 7. The main feature is that the SOC peaks are much smaller, broader, and less distinct than those in Fig. 2(a), which had $\chi = 1/3$. The one exception is that the peak at $h_1 = 0$ remains narrow because the relaxation process yields sites with $\mathbf{h} = \mathbf{0}$ exactly. The corresponding cumulative distribution function is shown in Fig. 8(b), from which it is seen that approximately 25% of the sites now have $h < 0$, due to the increasing dominance of diffusion over secular driving. In Fig. 8(c) we see that $D(s)$ is truncated at $s \approx 30$ and no longer has a clear power-law dependence on s, thus signifying the breakdown of the SOC state.

The results in Figs. 7 and 8 indicate that the SOC state breaks down as χ increases, beyond about 100. As χ increases, randomization due to addition of grains between avalanches is increasingly able to destroy the characteristic SOC correlations [e.g., as reflected in the peaks in $D(h_1)$] which would otherwise be established by successive avalanches. For $\chi \gg 100$ no SOC state is established; rather $\langle h_1 \rangle$ executes a random walk [a typical value of $|\langle h_1 \rangle|$ for $\chi = \infty$ is shown at $\chi = 1000$ in Fig. 7(a)], while $\sigma(h_1)$ approaches an asymptotic value (≈ 0.45 here) determined by the balance between driving and diffusive (rather than critical) transport to the boundaries of the system. Despite these comments, it is clear that the SOC state is extremely robust, with $\chi \gtrsim 100$ required before it is seriously affected by randomness.

B. Vector case

Figure 9 shows $\langle h_1 \rangle$, $\sigma(h_1)$, and $\sigma(h_2)$ for $D = 2$, $N = 100$, and $\Delta = 0.4$ for $0 \leq \mu \leq 0.32$ (as in Fig. 7, values for $\chi = \infty$ are plotted at $\chi = 1000$). The results for $\langle h_1 \rangle$ and $\sigma(h_1)$ are very similar to those in Fig. 7 and very similar comments apply here. In addition, we note that the breakdown in the SOC state occurs approximately when $\sigma(h_2)$ becomes comparable to $\langle h_1 \rangle$ and, beyond this point, $\sigma(h_1) \approx \sigma(h_2) > \langle h_1 \rangle$. This suggests that the SOC state is disrupted when the degree of driver-imposed disorder becomes significant, destroying the SOC correlations faster than they can be established by avalanches. This supports the remarks made in the previous subsection. The scaling $\sigma(h_2) \propto \chi^{1/2}$ [see Eq. (12)] breaks down for $\chi \gtrsim 10$ and $\sigma(h_2)$ saturates at ≈ 0.4 as $\chi \to \infty$. Arguments such as these imply that breakdown of the SOC state should occur somewhat sooner at large D where the disorder is greater, but the weak variations seen in Fig. 6 imply that it is not a strong effect.

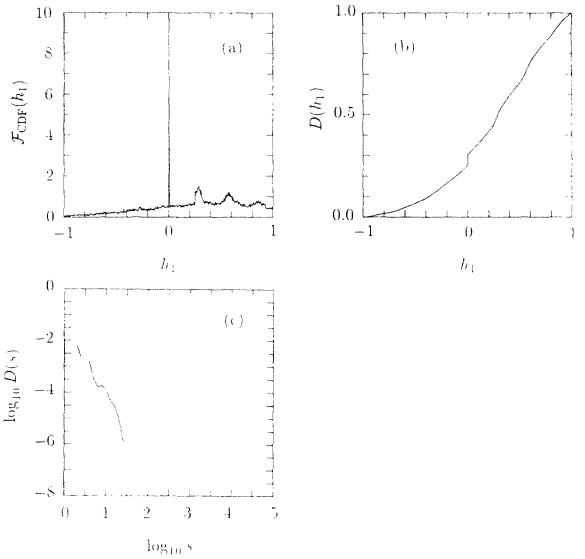

FIG. 8. Distributions of h_1 for $\chi = 107$, $N = 100$, and $D = 1$. (a) $D(h_1)$ vs h_1. (b) $\mathcal{F}_{\rm CDF}(h_1)$ vs h_1.

The above results are all for $N = 100$. Figure 3 shows that σ decreases with N, but that it tends to a nonzero limit as $N \to \infty$. Hence, we expect that SOC will persist to somewhat higher values of χ in larger systems, but that the boundary of SOC behavior will tend to a finite limit as $N \to \infty$.

V. SUMMARY AND DISCUSSION

This work has investigated the effects on self-organized criticality of introducing vector fields and randomness in

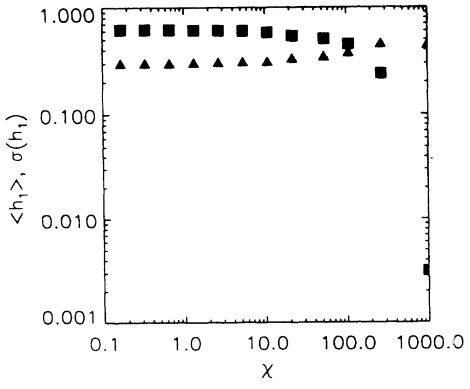

FIG. 7. Dependence of SOC state on χ for $N = 100$, $D = 1$, and $\Delta = 0.4$, showing $\langle h_1 \rangle$ (squares) and $\sigma(h_1)$ (triangles). Values for $\chi = \infty$ are shown at $\chi = 1000$.

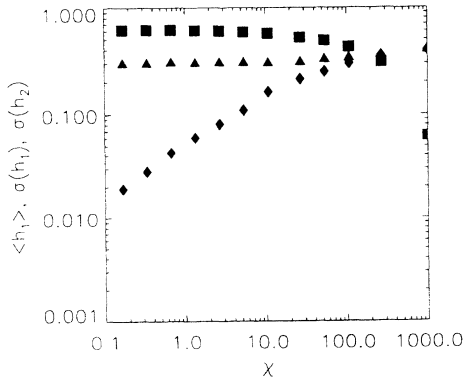

FIG. 9. Dependence of SOC state on χ for $N = 100$, $D = 2$, and $\Delta = 0.4$, showing $\langle h_1 \rangle$ (squares), $\sigma(h_1)$ (triangles), and $\sigma(h_2)$ (diamonds). Values for $\chi = \infty$ are shown at $\chi = 1000$.

the driving of the system. Our model displays SOC in both the scalar and vector cases. In the scalar case the scaling exponents and other properties of the SOC state are generally consistent with previous work on similar models, albeit toward the upper end of the range of previous values. The scaling of the total number of relaxations with the size shows a breakpoint at $a \approx 100$, with a significantly larger than s for larger sizes as multiple relaxations become more important. The height distribution displays four discrete peaks, as in Zhang's model [4], and the proportions of sites corresponding to each peak are consistent with previous analytic and numerical work on similar systems.

The behavior of vector-field SOC is dominated by the evolution of the secularly-driven field component, and is extremely similar to the scalar case. Other components are slaved to the principal one, with their RMS values scaling as $\chi^{1/2}$ for $\chi \lesssim 10$. SOC behavior is only weakly affected by the dimensionality D of the field, even for D as large as 20.

The effects of random driving are weak for $\chi \lesssim 100$ for both scalar and vector SOC. Beyond that point driver-imposed randomization destroys SOC correlations faster than they can be established via avalanches, causing the SOC state to break down. Breakdown appears to occur when the level of disorder imposed by the driving is approximately equal to the mean of h_1, the principal field component.

We conclude that the SOC state is extremely robust over a wide range of parameters, but that large degrees of disorder can nonetheless destroy it.

ACKNOWLEDGMENT

This work was supported by the Australian Research Council.

[1] P. Bak, C. Tang, and K. Wiesenfeld, Phys. Rev. Lett. **59**, 381 (1987).
[2] P. Bak, C. Tang, and K. Wiesenfeld, Phys. Rev. A **38**, 364 (1988).
[3] C. Tang and P. Bak, Phys. Rev. Lett. **60**, 2347 (1988).
[4] Y.-C. Zhang, Phys. Rev. Lett. **63**, 470 (1989).
[5] L. P. Kadanoff, S. R. Nagel, L. Wu, and S.-m. Zhou, Phys. Rev. A **39**, 6524 (1989).
[6] K. O'Brien, L. Wu, and S. R. Nagel, Phys. Rev. A **43**, 2052 (1991).
[7] S. S. Manna, J. Stat. Phys. **59**, 509 (1990).
[8] K. Christensen, H. C. Fogedby, and H. J. Jensen, J. Stat. Phys. **63**, 653 (1991).
[9] D. Dhar, Phys. Rev. Lett. **64**, 1613 (1990).
[10] T. Hwa and M. Kardar, Phys. Rev. Lett. **62**, 1813 (1989).
[11] S. N. Majumdar and D. Dhar, J. Phys. A **24**, L357 (1991).
[12] E. T. Lu and R. J. Hamilton, Astrophys. J. **380**, L89 (1991).